Cerebral Cortex, July 2020;30: 4257–4268

doi: 10.1093/cercor/bhaa053
Advance Access Publication Date: 26 March 2020
Original Article

ORIGINAL ARTICLE

Temporal Patterns of Emergence and Spatial Distribution of Sulcal Pits During Fetal Life

Hyuk Jin Yun[1,2], Lana Vasung[1,2], Tomo Tarui[3,4], Caitlin K. Rollins[5], Cynthia M. Ortinau[6], P. Ellen Grant[1,2] and Kiho Im[1,2]

[1]Fetal Neonatal Neuroimaging and Developmental Science Center, Boston Children's Hospital, Harvard Medical School, Boston, MA 02115, USA, [2]Division of Newborn Medicine, Boston Children's Hospital, Harvard Medical School, Boston, MA 02115, USA, [3]Mother Infant Research Institute, Tufts Medical Center, Tufts University School of Medicine, Boston, MA 02111, USA, [4]Department of Pediatrics, Tufts Medical Center, Tufts University School of Medicine, Boston, MA 02111, USA, [5]Department of Neurology, Boston Children's Hospital, Harvard Medical School, Boston, MA 02115, USA and [6]Department of Pediatrics, Washington University in St. Louis, St. Louis, MO 63110, USA

Address correspondence to Kiho Im, PhD, Fetal-Neonatal Neuroimaging and Developmental Science Center, Division of Newborn Medicine, Boston Children's Hospital, 300 Longwood Ave, Boston, MA 02115, USA. Email: kiho.im@childrens.harvard.edu.

Abstract

Sulcal pits are thought to represent the first cortical folds of primary sulci during neurodevelopment. The uniform spatial distribution of sulcal pits across individuals is hypothesized to be predetermined by a human-specific protomap which is related to functional localization under genetic controls in early fetal life. Thus, it is important to characterize temporal and spatial patterns of sulcal pits in the fetal brain that would provide additional information of functional development of the human brain and crucial insights into abnormal cortical maturation. In this paper, we investigated temporal patterns of emergence and spatial distribution of sulcal pits using 48 typically developing fetal brains in the second half of gestation. We found that the position and spatial variance of sulcal pits in the fetal brain are similar to those in the adult brain, and they are also temporally uniform against dynamic brain growth during fetal life. Furthermore, timing of pit emergence shows a regionally diverse pattern that may be associated with the subdivisions of the protomap. Our findings suggest that sulcal pits in the fetal brain are useful anatomical landmarks containing detailed information of functional localization in early cortical development and maintaining their spatial distribution throughout the human lifetime.

Key words: brain development, cortical sulci, fetal brain, first folds, sulcal pattern

Introduction

In the human brain, primary sulci are important landmarks of neurodevelopment. As a result of neurodevelopment, their folding pattern is highly complicated and variable across individuals (Ono et al. 1990). Despite the complexity and variability, sulcal pits, defined as locally deepest points of primary sulci, show a uniform spatial distribution in the human brain (Lohmann et al. 1999; Im et al. 2010; Meng et al. 2014; Auzias et al. 2015; Le Guen et al. 2017). As deep sulcal landmarks, sulcal pits are thought to be the first folds that appear during brain development and be related to the boundaries of major functional and cytoarchitectonic subdivisions (Welker, 1990; Zilles et al. 1997; Hasnain et al. 2001; Eickhoff et al. 2006; Fischl et al. 2008). The presence and distribution of the sulcal pits have also been associated with genetic effects. In monozygotic twin pairs, spatial distribution of sulcal pits was more similar compared to genetically unrelated individuals (Lohmann et al. 1999; Im et al. 2011b). A strong additive genetic effect on the presence and distribution

of the sulcal pits was found in a human pedigree cohort (Le Guen et al. 2017). Additionally, in a longitudinal study, the pit distribution was temporally consistent during the first 2 years after birth, despite dramatic cortical growth and increase in brain size (Meng et al. 2014). The reliability of sulcal pits was also investigated and identified that pit position is invariant to scan sessions, scanners, and surface extraction tools (Im et al. 2013a). These studies have supported that sulcal pits have a uniform distribution in the normal populations regardless of age and emphasized that they are reliable anatomical landmarks for human brain development. Based on the uniform pit distribution, sulcal pits have been employed in neuroimaging research investigating hemispheric asymmetry (Im et al. 2010; Meng et al. 2014; Auzias et al. 2015), human intelligence (Im et al. 2011a), and developmental disorders (Im et al. 2016, 2013b; Ortinau et al. 2019; Tarui et al. 2018).

It has been hypothesized that invariant sulcal pit distribution across individuals is influenced by a stable human-specific protomap of cytoarchitectonic areas. The protomap is thought to be associated with functional localization of the human cerebral cortex and consistently predetermined in early fetal stages under genetic controls (Rubenstein and Rakic, 1999; Piao et al. 2004; Rakic, 2004; O'Leary et al. 2007; Chen et al. 2012; Stahl et al. 2013; Miller et al. 2014). Although a protomap model could explain the uniform spatial distribution, there is a missing link in the evidence. To date, no one has explored the temporal uniformity of pit distributions from fetal to mature brains. Note that the second half of gestation is a crucial period of cortical folding in the human brain with temporal growth in terms of sulcal shape and relative position of sulci (Garel et al. 2003; Habas et al. 2012). After 22 gestational weeks (GW), there is little migration of neurons with dramatic changes of the human cerebral cortex (Mrzljak et al. 1988). Because of these dynamic changes, it needs to be determined whether the spatial distribution of sulcal pits in the fetal brain is temporally invariant across gestational ages and similar to the distribution in adult or neonatal brains. Temporal invariance of sulcal pit distribution would demonstrate that sulcal pits are lifelong anatomical landmarks from the initial stage of functional localization and provide important information to investigate early abnormalities in brain growth. Furthermore, it is well known that primary sulci have a specific timeline of emergence in typically developing (TD) fetal brains (Garel et al. 2003; Habas et al. 2012) which might be affected by rapid growth and regional expansion of functional areas (Welker, 1990; Ronan and Fletcher, 2015). The accurate timing of sulcal emergence has been used as a reliable index for estimating gestational age and detecting developmental disorders. However, several primary sulci frequently have two or more sulcal pits (Im et al. 2010; Meng et al. 2014; Auzias et al. 2015; Yun et al. 2019) that may be related to subdivisions of functional areas. Since measuring the timeline of cortical folding at a whole sulcal level cannot consider the difference of cortical expansion among the subdivisions, quantifying the timetable of pit emergence may provide more regional information of functional localization in human brain development.

To the best of our knowledge, the spatial and temporal patterns of sulcal pits in the fetal brain have not been investigated. In this paper, we employed 48 TD fetal brains between 22.0 and 32.0 GW, when the development of fetal cortex is characterized (Mrzljak et al. 1988), and a majority of primary sulci are emerging (Chi et al. 1977; Garel et al. 2001; Habas et al. 2012). First, we investigated spatial characteristics of sulcal pits. The position and spatial variance of sulcal pits of our 48 TD fetuses were compared to that of 148 healthy adults. We then divided the fetal cohort into three subgroups by GW and compared the position and spatial variance of sulcal pits among the subgroups. We hypothesized that the position and spatial variance of sulcal pits in the fetal brain are similar to those in adult brains and temporally invariant against GW. Second, we quantified the timing of emergence of sulcal pits. In contrast to pit distribution, timing of pit emergence may vary by different growth rate in each sulcal region. Thus, we hypothesized that sulcal pits show regionally different timings of emergence related to the subdivisions of the protomap.

Materials and Methods

Data and Image Acquisition

A total of 48 TD fetuses were included in this study (male/female, 30/18; age, 26.7 ± 2.9 GW [mean ± standard deviation (SD)], ranged from 22.0 to 32.0 GW) (Table 1). The use of the fetal subjects was approved by the Institutional Review Boards at Boston Children's Hospital (BCH) and Tufts Medical Center (TMC). TD subjects were identified from (1) a retrospective patient data at BCH and (2) prospective recruitment data for case control studies at BCH and TMC. All participants in the case control studies signed a written informed consent. For both data, we included TD fetuses with maternal age 18–45 years between 22 and 32 weeks of pregnancy and then excluded those who have multiple gestation pregnancies, dysmorphic features on ultrasound examination, other brain malformations or brain lesions, known chromosomal abnormalities, other identified organ anomalies, known congenital infections, and any abnormality on the fetal magnetic resonance (MR) imaging study. Fetal brain MR images were acquired on a Siemens 3 T Skyra scanner (BCH) or Phillips 1.5 T scanner (TMC) using a T2-weighted HASTE (half-Fourier acquisition single-shot turbo spin-echo) sequence with 1 mm in-plane resolution, FOV = 256 mm, time repetition = ~1.5 s (BCH) or 12.5 s (TMC), time echo = ~120 ms (BCH) or 180 ms (TMC), and slice thickness = 2–4 mm. After localizing the fetal brain, the HASTE scans were acquired multiple times in different orthogonal orientations for reliable image processing and analysis (scan time for acquisition of volumetric images was up to 20 min). A part of this multicenter TD subject data has been used in our prior studies, and there was no significant difference in accuracy of image processing and analysis across different scanners (Tarui et al. 2018; Yun et al. 2019).

In this study, we also employed a normal adult cohort to validate the spatial distribution of sulcal pits in our 48 TD fetuses. The cohort consisted of 148 normal adult subjects with 83 males and 65 females which have been used in previous studies (Lyttelton et al. 2009; Im et al. 2010). The age range of the adult subjects was from 18 to 44 years (mean ± SD: 25.0 ± 4.9). With a short questionnaire, there were 15 left-handed, 124 right-handed, and 9 unknown hand-dominant subjects. The subjects gave a written informed consent; the Research Ethics Committee of the Montreal Neurological Institute and Hospital approved the study, and their T1-weighted MR images (3D fast field echo scan with 140–160 slices, 1-mm isotropic resolution, TR = 18 ms, TE = 0 ms, flip angle = 30°) were acquired using a Phillips Gyroscan 1.5 T system.

Dividing Subgroups in the Fetal Cohort

For statistical analysis, we divided the TD fetal cohort into three subgroups by GW based on histogenic processes during fetal

Table 1 Demographic information of the fetuses used in this study

Subgroup	GW range [mean ± sd]	Sex (M/F)
G_{early} ($n = 16$)	22.0 ~ 24.7 [23.5 ± 0.8]	10/6
G_{mid} ($n = 16$)	25.1 ~ 28.0 [26.6 ± 0.9]	10/6
G_{late} ($n = 16$)	28.6 ~ 32.0 [30.1 ± 1.0]	10/6
All ($n = 48$)	22.0 ~ 32.0 [26.7 ± 2.9]	30/18

GW, gestational week; sd, standard deviation; M, male; and F, female.

brain development. Neuronal precursors migrate from proliferative zones to cortical plate in early fetal life. The majority of neurons reach their destination in the cortical plate by 22 GW (Bystron et al. 2008). After 22 GW, the development of fetal cortex is characterized by the growth of neurons, arborization of neuronal dendrites (Mrzljak et al. 1988), and appearance of primary sulci (Chi et al. 1977). Around 25 GW, the first thalamocortical axons start to relocate from the waiting compartment subplate into the cortical plate (Krsnik et al. 2017). Therefore, our first subgroup representing the early developmental period (G_{early}) spanned from 22.0 to 24.7 GW. From 25 GW, the development of the cerebral cortex is characterized by neuronal dendritic arborization, ingrowth of thalamocortical axons (predominantly during 25 and 26 GW), and the emergence of axonal pathways (Huang et al. 2009; Vasung et al. 2017, 2010). In the human brain, majority of sulcal roots are visible after 28 GW (Chi et al. 1977; Garel et al. 2001; Habas et al. 2012; Im and Grant, 2019). Thus, the second subgroup of development (G_{mid}) in our study spanned from 25.1 to 28.0 GW. From 28 GW, it is marked as the emergence of higher order cognitive functions (Draganova et al. 2005; Huotilainen et al. 2005). The subplate, which is essential in cortical development, is thickest and consistently visible until 32 GW and became progressively patchy (Judaš et al. 2013; Vasung et al. 2016; Diogo et al. 2019). Therefore, the third subgroup of development (G_{late}) in our study spanned from 28.6 to 32.0 GW. The demographic information of each developmental period is in Table 1.

MR Image Processing and Surface Reconstruction

For fetal MR image processing, we adopted our pipeline for surface extraction (Im et al. 2017; Tarui et al. 2018; Yun et al. 2019). Using a slice to volume super-resolution technique, we combined multiple 2D slices of fetal brain MR images to create a motion-corrected 3D volume with 0.75 mm isotropic resolution (Kuklisova-Murgasova et al. 2012). Then, the cortical plate was segmented by a semiautomatic approach based on voxel intensities. Spatial smoothing was performed in the segmented inner volume of the cortical plate using 1.5 mm full width at half-maximum (FWHM) kernel to minimize the noise. Using the smoothed inner cortical plate, the hemispheric (left and right) triangular surface meshes of the cortical plate were automatically extracted by a function "isosurface" in MATLAB 2016b (MathWorks Inc.). The surface models were geometrically smoothed using Freesurfer (https://surfer.nmr.mgh.harvard.edu) to eliminate noise and small geometric changes. To have vertex-wise correspondence among the individual surfaces, we aligned the smoothed cortical surfaces using a 2D sphere-to-sphere warping method (Robbins, 2004; Boucher et al. 2009). To minimize the technical errors of the warping method, we selected a 28 GW template surface as a registration target which is smooth but has all the primary sulci. The template surface was extracted from T2 MRI volume templates that were generated and published using a different fetal cohort from ours (Serag et al. 2012; Yun et al. 2019). High accuracy of surface registration between fetal brains has been reported in our prior study (Yun et al. 2019).

Structural MR images of the adult cohort were processed by CIVET pipeline from Montreal Neurological Institute (MNI, http://www.bic.mni.mcgill.ca). MR images were spatially aligned into the MNI 152 average template using a linear transformation after intensity nonuniformity correction (Collins et al. 1994; Sled et al. 1998). Then, the brain tissues were classified into gray matter, white matter, cerebrospinal fluid, and background using an advanced neural net classifier (Zijdenbos et al. 1996). Individual inner cortical surfaces were extracted by deforming a spherical mesh onto the boundary between white and gray matter (MacDonald et al. 2000). The reconstructed surfaces were aligned to a surface group template (Lyttelton et al. 2007) using surface registration (Robbins, 2004; Boucher et al. 2009).

Extracting Sulcal Pits and Generating Cluster Map

To extract sulcal pits and their catchment basins, mean curvature, sulcal depth, and surface area were measured on the cortical surfaces. The surface area was computed using an area of Voronoi region of each vertex on the cortical surface (Meyer et al. 2003). Mean curvature is defined as the angular deviation from a patch around each vertex, and its sign indicates inwardly folded (negative) or outwardly folded (positive) regions (Meyer et al. 2003). We calculated sulcal depth on the cortical surface using adaptive distance transform searching shortest path from the convex hull to the cortical surface (Yun et al. 2013). Mean curvature and sulcal depth were transformed to the fetal and adult template surfaces using surface registration, respectively. We then smoothed mean curvature and sulcal depth on the template surfaces with 10 mm FWHM Gaussian smoothing kernel (Chung et al. 2003) which was previously proven to be a proper kernel size to reliably extract sulcal pits and basins (Im et al. 2016, 2013a, 2010; Tarui et al. 2018; Yun et al. 2019). Smoothing on the template surface provides the same spatial extent of smoothing kernel size that reduces brain size effects across individuals.

For each fetal and adult cohort, we applied different measures to extract pits and basins. The cortical folding pattern in the fetal brain is smooth, and the deepest regions defined by mean curvature and sulcal depth are similarly located (see Supplementary Fig. S1). However, some early cortical sulci in the fetal brain are too small and shallow to be identified by sulcal depth after smoothing, whereas mean curvature is more sensitive for extracting sulcal pits on the fetal cortical surface. Thus, we used mean curvature to extract sulcal pits in the fetal brain. From the vertex with the most negative mean curvature, which represents the deepest part of the sulci, a watershed

flooding algorithm was applied for extracting sulcal pits and basins (Im et al. 2010). We applied merging criteria to remove noisy sulcal pits which were generated by minor geometric variation of cortical surfaces. For the criteria, three thresholds were applied—area of the basin [*ThrA*], geodesic distance between two pits [*ThrD*], and ridge height [*ThrR*]. Since the thresholds were calculated by geometrical features, they were sensitive to individual brain size. Thus, we used the thresholds that were normalized by considering fetal brain size ($ThrA = 0.0004 * SurfaceArea$, $ThrD = 2.165 * ThrA^{0.542}$, and $ThrR = 0.25 * AverageCurvature$). See Yun et al. 2019, for a more detailed explanation of the method for determining the thresholds. Then the watershed flooding was only processed in the vertices with negative mean curvature to prevent extracting pits and basins in nonsulcal regions.

For adult brains, we extracted pits and basins using sulcal depth. We found optimal thresholds for the adults in the same way as our previous study (Yun et al. 2019): $ThrA = 0.0004 * SurfaceArea$, $ThrD = 4.019 * ThrA^{0.374}$, and $ThrR = 0.25 * AverageDepth$. Details for normalizing the thresholds and its reliability are described in Supplementary Methods and Supplementary Figure S2. The watershed flooding was terminated when the water reached the vertex which has a smaller depth than average sulcal depth.

To define consistent regions of sulcal pits across individuals, density and cluster maps were generated in each fetal and adult cohort. We smoothed all the sulcal pits with 10 mm FWHM kernel, preserving the value of pits as maximum of 1 (Im et al. 2010) and averaged smoothed sulcal pits in each cohort to generate density map. High density indicated that the sulcal pits were extracted in a large number of subjects into these regions with small spatial variation. The density maps of the fetal and adult cohorts are shown in Figure 1A and C. In the fetal cohort, we separated density maps by subgroups (G_{early}, G_{mid}, and G_{late}). To check the reliability of the density map against different target template surfaces, we registered sulcal pits to 25 and 31 GW template surfaces and found that there was no difference by selecting target surfaces (see Supplementary Fig. S3).

Based on the density maps, we segmented cluster maps. Applying the same merging thresholds for each cohort, we segmented the clusters with high density in each cohort using the watershed algorithm described above. We manually selected clusters of primary sulci in fetal cluster map and then selected corresponding clusters in adult cluster map (Fig. 1B and D) following our previous studies (Im et al. 2010; Yun et al. 2019). Since there are some clusters with the absence of sulcal pits in early fetuses, we performed a supplementary analysis that segmented sulcal pit clusters in each subgroup to compare their boundary patterns. In Supplementary Figure S4, the number of clusters is different among subgroups; however, the cluster boundary patterns in existing clusters are largely similar to each other. This similarity demonstrated that the cluster map of the fetal cohort represents spatial distribution of sulcal pit of the fetal subjects. We also assumed some clusters without sulcal pits in early fetuses are potential regions where sulcal pits may emerge in the later fetal life.

Dimension Reduction of Coordinates of Sulcal Pits

Sulcal pits are in 3D coordinate system based on the location of vertices in the cortical surfaces (Fig. 2A). Since the 3D coordinates consist of many factors such as relative position of sulci, brain size, and sulcal deepening, they might vary by GW and gyrification (see Supplementary Fig. S5). To statistically analyze spatial distribution of sulcal pits, it is necessary to convert the coordinates with only positional information along the deep sulcal regions. Because the topology of the surface model is same as a sphere, sulcal pits in the fetal brain were converted to a spherical coordinate system (Fig. 2B). With a constant radial distance, the spherical coordinate system reduces the 3D coordinates to 2D, removing brain size effect across fetuses. The 2D coordinates of sulcal pits consisted of the polar (θ) and azimuth (φ) angles, but they are inappropriate for evaluating their positional information on cortical surfaces (Tao et al. 2002). Thus we constructed a tangent plane as an orthogonal (u, v) coordinate system of each cluster whose origin is the average position of the pits belonging to the cluster (Tao et al. 2002; Im et al. 2010). In case multiple sulcal pits per subject are extracted in a cluster, only one pit which is more closely located to pit distribution of other subjects was selected (Im et al. 2011a). The selected sulcal pits in the cluster were projected onto the tangent plane and shown in Figure 2C. This 2D coordinates is able to show spatial distribution of sulcal pits in the deep sulcal regions. In most clusters, sulcal pits were distributed similar to a long ellipsoid (Fig. 2C) because the sulcal pits are located along sulcal fundi. Thus, we applied a principal component analysis (PCA) of the sulcal pits on 2D tangent plane and converted them to 1D coordinates along with the first principal component (Fig. 2C). The first principal component explained over 80% of spatial variance of sulcal pits in the most clusters (see Supplementary Table S1); therefore, we assume the 1D coordinates represent the relative position of sulcal pits along the deep sulcal regions. In this study, all the statistical analyses of pit distribution were performed using the 1D coordinates.

Data Analysis

Comparison of Sulcal Pit Distribution Between the Fetal and Adult Brains

We visually compared the spatial distribution of the sulcal pit clusters between the fetal and the adult cohorts. In this comparison, we focused on the cluster boundaries and the number of clusters in primary sulci. We aligned adult cluster boundary map to the fetal surface template using surface registration (Robbins, 2004; Boucher et al. 2009) and compared the boundaries of corresponding clusters. In the fetal cohort, we evaluated the frequency of sulcal pits by calculating a percentage of fetuses in which a specific sulcal pit was identified. Clusters with high frequency in the G_{early} indicated that they emerge early in fetal life and vice versa. We visually compared the frequency, density, and SD of 1D coordinates of sulcal pits in the clusters among the three fetal subgroups.

Spatiotemporal Distribution of Sulcal Pits in the Fetal Brain

We analyzed the spatiotemporal distribution of sulcal pits using two approaches. First, positional invariance of sulcal pits was tested using 1D coordinates which represent the location of sulcal pits in each cluster. The difference in the position of sulcal pits among the subgroups was investigated using a Kruskal–Wallis test for each cluster. Insignificance of the test indicates the spatial uniformity of sulcal pits among the subgroups—in other words, there is no positional displacement of the first cortical folds during brain development. Second, we examined

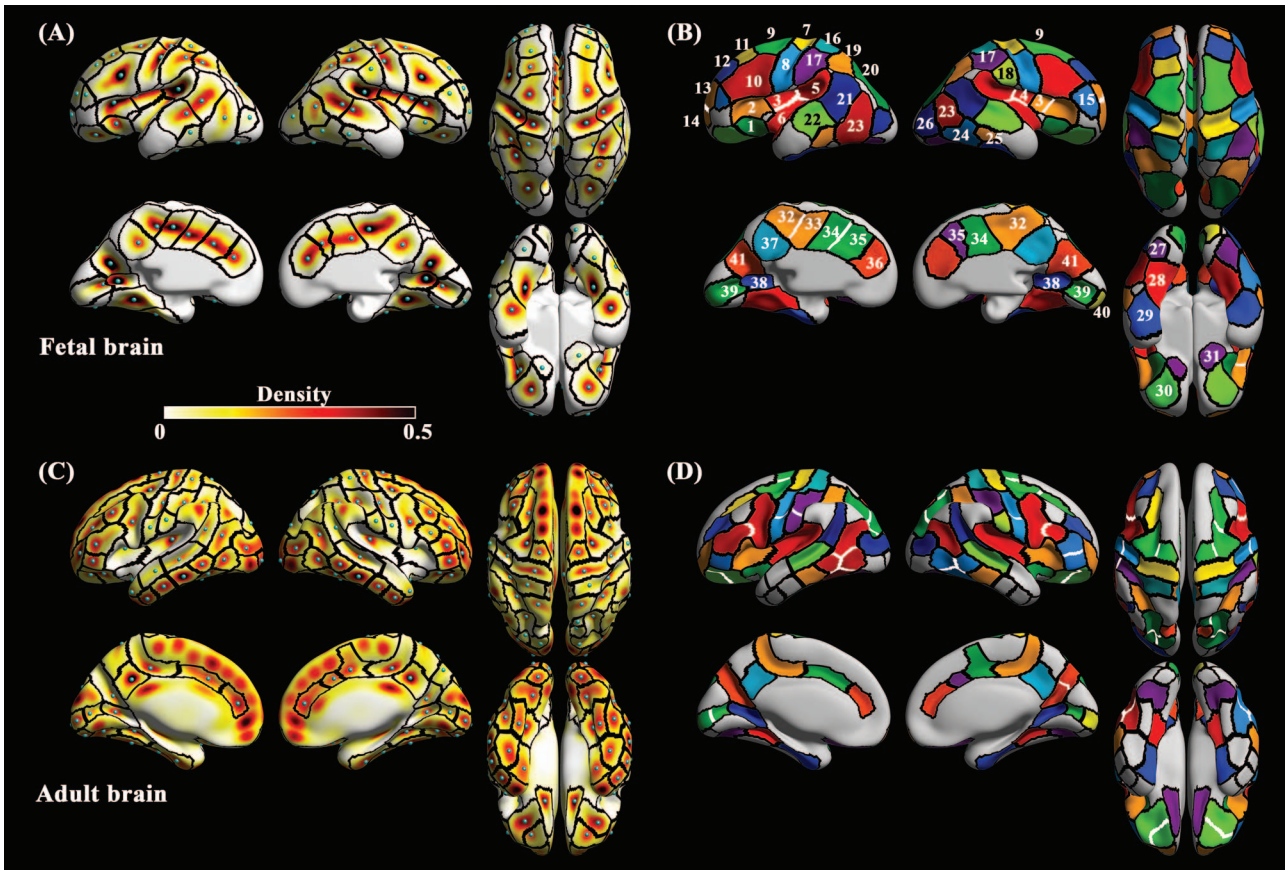

Figure 1. The density and cluster maps of sulcal pits in the fetal and adult cohorts. (*A*) density and (*B*) cluster maps generated by all the subjects in the fetal cohort. The numbers in clusters correspond to the sulcal labels (1, Sylvian fissure [SF] *a*; 2, SF *b*; 3, SF *c*; 4, SF *d*; 5, SF *e*; 6, SF *f*; 7, central [CS] *a*; 8, CS *b*; 9, precentral [PreCS] *a*; 10, PreCS *b*; 11, superior frontal [SFS]; 12, middle frontal [MFS] *a*; 13, MFS *b*; 14, MFS *c*; 15, inferior frontal [IFS]; 16, postcentral [PostCS] *a*; 17, PostCS *b*; 18, PostCS *c*; 19, intraparietal [IPS] *a*; 20, IPS *b*; 21, superior temporal [STS] *a*; 22, STS *b*; 23, inferior temporal [ITS] *a*; 24, ITS *b*; 25, ITS *c*; 26, lateral occipital [LOS]; 27, collateral [ColS] *a*; 28, ColS *b*; 29, ColS *c*; 30, orbital [OrbS]; 31, olfactory [OlfS]; 32, cingulate [CingS] *a*; 33, CingS *b*; 34, CingS *c*; 35, CingS *d*; 36, CingS *e*; 37, subparietal [SPS]; 38, calcarine [CalS] *a*; 39, CalS *b*; 40, CalS *c*; 41, parieto-occipital [POS] sulcus). In the adult cohort, (*C*) density and (*D*) cluster maps are shown. Black lines on the maps represent the boundaries of clusters. Light blue spheres on the density maps indicate the peak position of density. White lines represent the boundaries which were not shown in the other cluster map. Corresponding clusters between fetal and adult cohorts have same color codes.

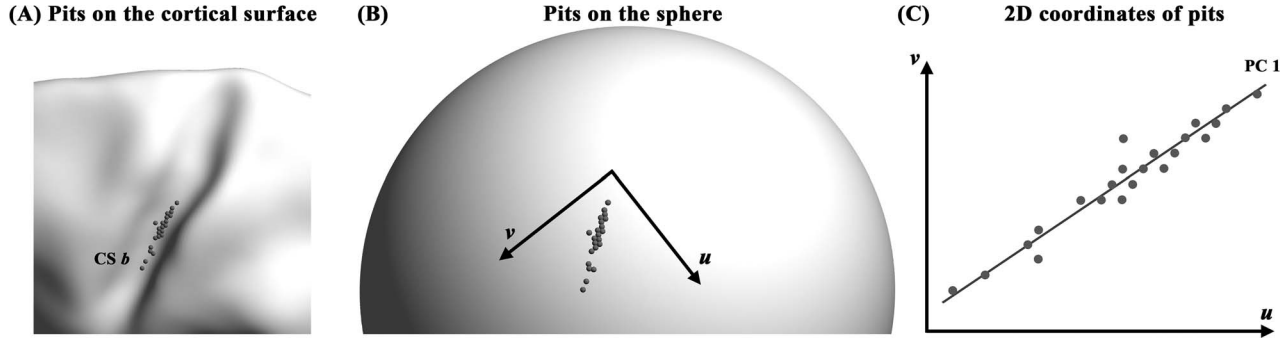

Figure 2. Dimension reduction of coordinates of sulcal pits. (*A*) 3D pit coordinates on the cortical surface (gray spheres) are converted to (*B*) the 2D spherical coordinates. (*C*) Sulcal pits on the spherical coordinate system are projected to tangential plane (gray circles) which has an orthogonal coordinate system (u, v). PCA is performed on 2D coordinates on tangent plane and converted them to 1D coordinates along with the first principal component (PC1, line). Cluster name corresponds to those of Figure 1.

the similarity of the spatial variance of sulcal pits across the subgroups. Pearson's correlation analysis was performed with the SD values of sulcal pit positions from all clusters in the whole brain between two subgroups. We excluded the clusters where the SD could not be calculated due to the small number of sulcal pits (<2). High correlation coefficient indicates that the pattern of the spatial variances across the clusters is temporally similar against dynamic brain growth with GW. Between the

fetal subgroups and adult cohort, we selected corresponding clusters and performed a correlation analysis with SD values of the clusters. In all the statistical analysis, we set the significance level at the corrected p value of 0.05 after false-discovery-rate (FDR) correction.

Timing of Emergence of Sulcal Pits in the Fetal Brain

To estimate the timing of pit emergence in each cluster, the presence of pits was counted as binary variables (1 when the pits were present and 0 when absent) for each subgroup of the fetal cohort. For subjects who had more than one sulcal pit in the cluster, we also counted them as 1. Then we generated crosstab table with the variables and performed chi-square tests to examine if there is a rapid change of pit presence between G_{early} and G_{mid} and between G_{mid} and G_{late}. The significant change between the subgroups indicates that there is a specific timing of emergence of sulcal pits. The timing and frequency were mapped on the template surface.

Results

Spatial Distribution of Sulcal Pits in the Fetal and Adult Brains

We segmented 76 fetal clusters (37 for left and 39 for right hemisphere) and 116 adult clusters (58 for each hemisphere) (Fig. 1B and D). We visually examined the number of clusters in each sulcus and the similarity of cluster boundaries between the fetal and adult cohorts. As can be seen in Figure 1, clusters in the fetal brain showed correspondence to those in the adult brain in terms of position. Boundaries of corresponding clusters between the fetal and adult maps showed a similar pattern specifically in bilateral central sulcus (CS) *a*, postcentral sulcus (PostCS) *a*, superior temporal sulcus (STS), subparietal sulcus (SPS), lateral occipital sulcus (LOS), olfactory sulcus (OlfS), left parieto-occipital sulcus (POS), and calcarine sulcus (CalS) *a* (see Supplementary Fig. S6A). However, there were some differences in detail. First, some clusters were not identified in the fetal brain. Clusters belonging to the temporal lobe such as anterior parts of STS and inferior temporal sulci (ITS) in the adult brain were not identified in the fetal brain. Some fetal clusters corresponded to two or more adult clusters in the bilateral CS, precental (PreCS), intraparietal (IPS), orbital (OrbS), ITS, left PostCS, left CalS, and right POS. On the contrary, the bilateral Sylvian fissure (SF) and left cingulate sulcus (CingS) showed an increased number of clusters in the fetal brain. Second, pit frequency in the fetal cohort is lower than that of the adult cohort. The clusters belonging to CS, PreCS, SFS, and MFS showed a large difference in frequency between the cohorts (Fig. 3A and Supplementary Fig. S6B). The fetuses showed near 0.5 of frequency, while adults showed over 0.9 of frequency in those clusters. The frequency pattern of G_{late} was similar to that of the adults.

Temporal Invariance of Spatial Distribution of Sulcal Pits

The increase and decrease in density and SD were visually confirmed in Figure 3B and C, respectively. Density showed a dynamic increase from G_{early} to G_{late} which is similar to the frequency pattern (Fig. 3A). Although dynamic changes in density were visually found in most of the cluster, the Kruskal–Wallis test showed no significant difference in pit position among the subgroups (see Supplementary Fig. S7). Some clusters with low pit frequency in the fetal cohort (the bilateral middle frontal sulcus (MFS) c, OlfS, LOS, left inferior frontal sulcus (IFS), left MFS *b*, left collateral sulcus (ColS) *a*, right ITS c, and right CalS c) were excluded in the Kruskal–Wallis test. On the contrary to the density changes (Fig. 3B), a relatively small decrease of SD among the subgroups was shown, but similar spatial pattern of SD across the whole cortex were found among subgroups (Fig. 3C). For example, the left SF *c*, left STS *a*, left ITS *a*, left PostCS *b*, right SPS, and right CingS *a* and *c* showed consistently higher SD than other clusters across all fetal subgroups. Pearson's correlation tests showed significant positive correlations of the SD of sulcal pit positions between G_{early} and G_{mid} [$r = 0.59$, $P < 0.001$], G_{early} and G_{late} [$r = 0.50$, $P = 0.001$], G_{mid} and G_{late} [$r = 0.70$, $P < 0.001$] (Fig. 4A–C). SD values of the adult cohort also showed significant correlation with G_{mid} [$r = 0.55$, $P < 0.001$] and G_{late} [$r = 0.31$, $P = 0.019$] (Fig. 4E and F). G_{early} showed insignificant correlation of SD with adults, but it showed a positive trend (Fig. 4D). Overall patterns of SD in the fetal and adult cohorts were shown in Figure 3C and Supplementary Figure S6C, respectively.

Temporal Pattern of Sulcal Pit Emergence

Frequency of the clusters in the fetal brain were shown in Figure 3A. The increase of frequency from G_{early} to G_{late} was found in all the clusters. The statistics of frequency change showed a diverse pattern in several fetal clusters (Fig. 5). A significant increase in the frequency between G_{early} and G_{mid} was found in several clusters such as the bilateral CS *a* and *b*, PreCS *a*, PostCS *b*, CalS *b*, OrbS, left STS *b*, left IPS *a*, left STS *b*, and right POS. From G_{mid} to G_{late}, the bilateral middle frontal sulcus (MFS) *a*, IPS *b*, left MFS *b*, right PreCS *a*, right IPS *a*, right ITS *a* and *b*, right LOS, and right CalS *b* showed significant increase of frequency. Interestingly, significant increases of frequency in the right PreCS *a* and right CalS *b* were found in both periods. In other clusters, no statistically significant frequency change was found. Some clusters with high frequency (>0.3) in G_{early} such as the bilateral SF *a*, *b*, *c*, *d*, *e*, and *f*; CingS *a*, *b*, *c*, *d*, and *e*; STS *a*; PreCS *b*; SPS; CalS *a*; ColS *b* and *c*; left POS; and right STS *b* showed insignificant changes of frequency. The frequency changes in these clusters may not be captured in our fetal cohort, since they generally develop earlier than 22 GW (Garel et al. 2001; Habas et al. 2012), which is the earliest age in our fetal cohort. Furthermore, the other clusters also showed insignificant frequency change: the bilateral OlfS, MFS *c*, ColS *a*, IFS, PostCS *a*, ITS *c*, left LOS, left superior frontal sulcus (SFS), left ITS *a*, right PostCS *c*, right MFS *b*, and right CalS *c*. The detailed frequency changes among the fetal subgroups and the adult cohort were shown in Supplementary Figure S8.

Discussion

In this study, we aimed to characterize spatial distribution and emergence of sulcal pits during fetal brain development. The findings support our hypothesis that the position and spatial variance of the sulcal pits in the fetal brain show similar pattern compared to those in the adult brain and temporal uniformity among the fetal subgroups against dynamic brain development; and the timing of pit emergence is regionally diverse across the fetal clusters.

We found that there was spatially similar correspondence of the clusters between the fetal and adult brains. The boundaries of clusters were similar in each sulcus, but the number of

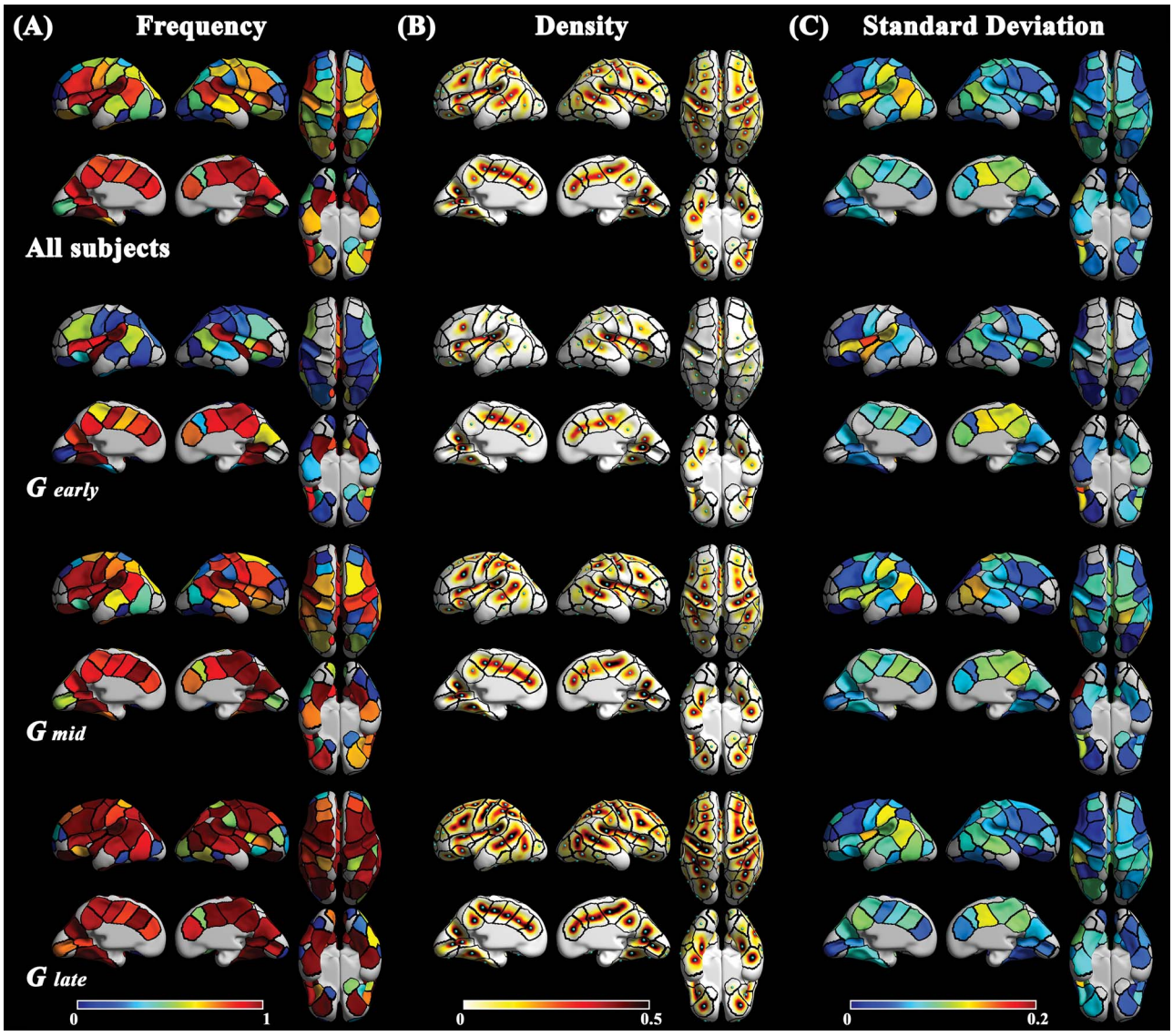

Figure 3. (*A*) Frequency, (*B*) density, and (*C*) standard deviation of the position of sulcal pits in the fetal brain. Black lines indicate the boundaries of clusters generated by all the subjects from fetal cohort. Light blue spheres on the density maps indicate the peak position of density. Each row represents the group used to generate the maps (from top to bottom: all fetal subjects, G_{early}, G_{mid}, and G_{late}).

clusters was different in most of the sulci. Fetal brains showed smaller numbers of clusters than adult brains in the bilateral CS, PreCS, IFS, IPS, STS, ITS, OrbS, left CalS, left PostCS, and right POS. This indicates that clusters in those sulci may develop and divide later in fetal life. Interestingly, fetuses had more clusters in the bilateral SF and left CingS, although they emerge early during fetal life.

The first cortical sulci are thought to fold during the early stage of cortical growth and have a stable number, position, and orientation. Previous studies have reported that sulcal pits are found in similar positions in the mature brain and they partially showed that sulcal pits represent the first cortical sulci (Lohmann et al. 2008; Im et al. 2010; Meng et al. 2014; Auzias et al. 2015; Le Guen et al. 2017; Im and Grant, 2019). In this study, we found the invariance of pit position among the fetal subgroups. The temporally invariant position of sulcal pits in the fetal brain despite dynamic growth during the second half of gestation supports stable position of the first cortical sulci. This demonstrates that sulcal pits are landmarks which have developmental information of the human brain. Some sulci had clusters with relatively higher spatial variance of the sulcal pits compared to others. The clusters belonging to the SF, STS, PostCS, ITS, ColS, SPS, and CingS are also shown to have a high spatial variability in the adult brain due to several sulcal branches. For example, in the adult brain, connections of the marginal ramus with the CingS with paracentral sulcus are highly variable, and the posterior parts of the ITS display a highly interrupted pattern (Ono et al. 1990). In the clusters in SF, their high spatial variance can be explained by hemispheric difference and density patterns. These clusters might be divided into two clusters in later fetal life, because their corresponding clusters in the other hemisphere were already divided, and the position of their peak density was relatively variable among the subgroups. Among the fetal subgroups, the strong

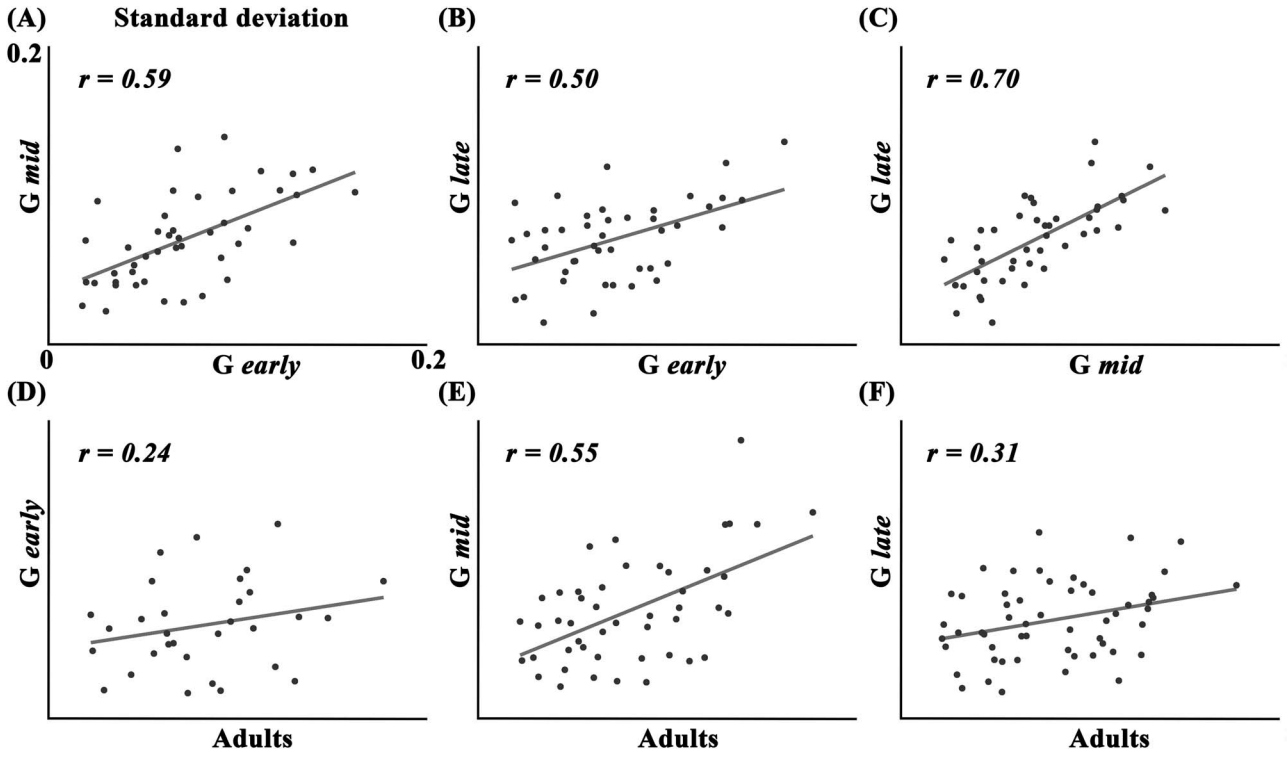

Figure 4. Correlation of standard deviation of pit coordinates between subgroups. (*A*) G_{early} and G_{mid}, (*B*) G_{early} and G_{late}, (*C*) G_{mid} and G_{late}, (*D*) G_{early} and adults, (*E*) G_{mid} and adults, and (*F*) G_{late} and adults.

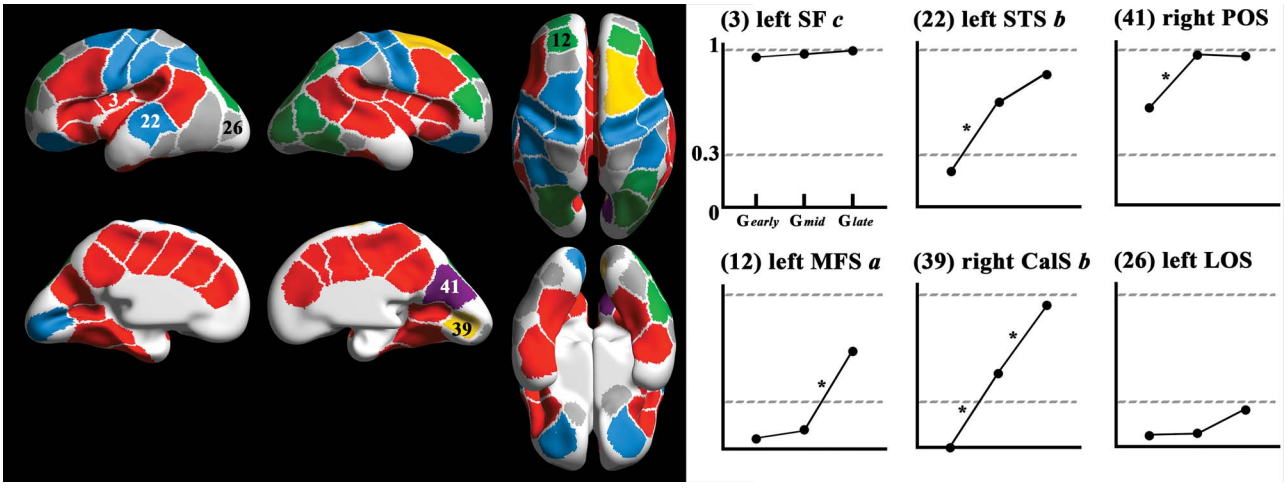

Figure 5. Cluster-wise results of pit frequency and chi-square tests. The colors in the clusters on the surface (left) indicating changes of pit frequency among fetal subgroups and examples of changes of frequency in six clusters are provided (right). Cluster indices and names correspond to those of Figure 1. Colors of the clusters represent the statistics of frequency change. Red: pit frequency in G_{early} over 0.3 and no significant change between subgroups. Light blue: significant increase of pit presence using chi-square test from G_{early} to G_{mid}. Purple: both high frequency in G_{early} (>0.3) and significant increase of pit presence using chi-square test from G_{early} to G_{mid}. Green: significant increase of pit presence using chi-square test from G_{mid} to G_{late}. Yellow: significant increase of pit presence using chi-square test from G_{early} to G_{mid} and from G_{mid} to G_{late}. Gray: low frequency in G_{early} (<0.3) and no significant change. *: significant change of pit presence (FDR corrected $P < 0.05$) between two subgroups.

correlations of SD indicate spatial variance of sulcal pits is temporally similar. The results support that spatial variance of sulcal pits is determined in early fetal life; it may be linked to regional-specific characteristics in each subdivision of the protomap; and spatial variance of sulcal pits may be maintained throughout human lifetime. Finally, our findings demonstrate that sulcal pits contain spatial information of position and its variance of the first sulcal folds that are important landmarks to investigate human brain development and functional localization.

The increasing pattern of pit frequency was observed with GW, although pit frequency was variant across clusters. This pattern indicates that there is a specific period of pit emergence

in each cluster. These results are supported by previous studies using in vivo fetal MR images, which observe sulcal emergence to occur during specified times of fetal brain development (Chi et al. 1977; Garel et al. 2001; Fogliarini et al. 2005; Dubois et al. 2008; Habas et al. 2012). Also, we found three different emerging patterns across the clusters. First, we found that sulcal pits in some clusters showed high frequency (>0.3) in G_{early}. These clusters were situated in the center of the cortical regions on the lateral and medial view (Fig. 5). Furthermore, they belong to the borders of the limbic cortex (i.e., the CingS with its marginal branch, SPS, anterior parts of the CalS, POS, ColS without the anterior paraolfactory and rhinal sulci) (Duvernoy et al. 1992; Donkelaar et al. 2018) and encircled the bilateral SF (the SF, STS *a*, and PreCS *b*). Second, the increase of pit frequency between G_{early} and G_{mid} was found in the clusters that are located peripherally, i.e., further from the limbic and primary visual cortex. These clusters are predominantly belonging to the dorsolateral parts of the brain (the bilateral CS *a*, PreCS *a* and PostCS *b*, right IPS *a*, right ITS *a*), primary visual cortex (the bilateral CalS *b*, right POS), and sulci near SF (the bilateral OrbS, CS *a*, and left STS *b*). Third, the other clusters, where sulcal pits may emerge in later fetal life, were observed in more peripheral parts of the brain than those above (the bilateral PostCS *c*, ColS *a*, ITS, LOS, IFS, MFS, OlfS, and right CalS *c*). Interestingly, these three emerging patterns roughly reflect the phylogenetic and functional localization of the cerebral cortex. The phylogenetically older allocortex, which does not undergo an ontogenetic six-layer stage during the development (Brodmann, 1909; Zilles, 2018), is centrally situated on the medial (the piriform, presubicular, entorhinal, subgenual, supracallosal, and retrosplenial cortices) and lateral parts (the anterior insular cortex) of the brain. In contrast to the allocortex, the heterotypic isocortex undergoes significant changes in the organization of cortical layers and diverges considerably from the homogenous six-layer cerebral cortex that is shown in many cortical areas during the third trimester of development (Brodmann, 1909). The areas of the cortex that are composed out of heterotypic isocortex are the primary visual area in the CalS (area 17), granular insular cortex in the posterior part of the SF, and primary motor cortex in the precentral gyrus (area 4) (Marin-Padilla, 1970). Besides the allocortex and heterotypic isocortex, the primary somatosensory regions such as the primary sensory and auditory cortices are also centrally situated on the lateral parts of the brain. Thus, the allocortex, heterotypic isocortex, and primary somatosensory cortex correspond to the clusters with high pit frequency (>0.3) in G_{early}. The clusters peripherally situated (e.g., MFS and ITS) showed that pit emerged in later developmental period (G_{mid} or later). Our results indicate there is a gradient of timing of cortical maturation from the central to peripheral regions (through the phylogenetically older and functionally simpler cortical areas), which might not be captured by the timing of whole sulcal emergence.

Although the current study showed meaningful results of spatial distribution and emergence of sulcal pits in the fetal brain, there are some limitations that should be investigated in the future study. First are the different patterns of the cluster boundaries in the bilateral SF and left CingS between the cohorts. Previous studies with a large sample of human brains showed individual variability with different morphological types (continuity, location and number of vertically oriented branches, and presence of paracingulate sulcus) of the CingS (Ono et al. 1990; Paus et al. 1996). We also found lower explanation percentages of the first principal components of clusters in the left CingS that may represent intersubject variability (see Supplementary Table 1). Thus, it would be worth to divide types and analyze the spatial distribution of sulcal pits separately. To divide the types, longitudinal information may need to divide the types of the CingS which cannot be captured in our early and smooth fetal brains. In contrast to the CingS, the dissimilar boundaries of the SF can be explained by a difference in geometrical features used for identification of sulcal pits. While positions of sulcal pits extracted by mean curvature and sulcal depth are similar, some sulcal pits in SF are not matched between mean curvature and sulcal depth (see Fig. 1*A* and Supplementary Fig. S1*B*). The density and cluster map generated by sulcal depth shows a similar pattern to the adult density map in the SF, while the patterns of cluster boundaries in the other regions are similar to those in the fetal brain (see Supplementary Fig. S1*B*). Thus, finding a reliable geometrical feature for pit extraction would help clarify the difference of cluster boundaries in SF between the cohorts. Second, the lack of longitudinal fetal brain MR images is a shortcoming of this study. While our findings demonstrated temporal invariance of spatial distribution of sulcal pits during fetal life, testing longitudinal data would clearly confirm this. Therefore, longitudinal imaging of fetal brains should be analyzed in the further works. Third, smoothness of surface is a major factor for calculating mean curvature, and it may affect the number of sulcal pits (Cachia et al. 2003). Although our approach has been used in previous studies (Tarui et al. 2018; Ortinau et al. 2019; Yun et al. 2019) and extracted reliable number of sulcal pits, it is necessary to optimize the smoothness of surfaces for fetuses in the future study. Last, we used constant FWHM kernel size for fetuses and adults. Because the fetal template surface is smaller than the adult one, it may cause a problem when comparing measures between two cohorts. Although we only performed visual comparison between the fetal and adult cohorts, selecting and applying optimal sizes of smoothing kernel to compare fetal and adult brains is needed for the future statistical approaches.

In summary, this article has three main contributions. First, we found the position and spatial variance of sulcal pits show similar patterns between the fetal and adult cohort. Second, we provided statistical results showing that the position and spatial variance of sulcal pits are temporally settled in early fetal life against dynamic brain growth. Last, we quantified the timing of pit emergence in each cluster and parcellated them into three emerging patterns related to protomap subdivisions under genetic controls. Based on the findings, we suggest that sulcal pits in the fetal brain have the potential to be useful landmarks for analyzing the topological features for the folding pattern and for detecting altered cortical maturation in early stages of neurodevelopment.

Supplementary Material

Supplementary material can be found at *Cerebral Cortex* online.

Funding

Eunice Kennedy Shriver National Institute of Child Health and Human Development of the National Institutes of Health (NIH) (grants R21HD094130 and U01HD087211); National Institute of Biomedical Imaging and Bioengineering of the NIH (grant R01EB017337); the National Institute of Neurological Disorders and Stroke of the NIH (grant K23NS101120); American Heart Association (grant 19IPLOI34660336); and Swiss National Science

Foundation (grant P300PB_167804). The content is solely the responsibility of the authors and does not necessarily represent the official views of the NIH.

Conflict of Interest

None declared.

References

Auzias G, Brun L, Deruelle C, Coulon O. 2015. Deep sulcal landmarks: algorithmic and conceptual improvements in the definition and extraction of sulcal pits. *NeuroImage*. 111:12–25. doi: 10.1016/j.neuroimage.2015.02.008.

Boucher M, Whitesides S, Evans A. 2009. Depth potential function for folding pattern representation, registration and analysis. *Med Image Anal*. 13:203–214. doi: 10.1016/j.media.2008.09.001.

Brodmann K. 1909/2006. Localization in the Cerebral Cortex, translated by Garey LJ. New York: Springer.

Bystron I, Blakemore C, Rakic P. 2008. Development of the human cerebral cortex: boulder committee revisited. *Nat Rev Neurosci*. 9:110–122. doi: 10.1038/nrn2252.

Cachia A, Mangin J-F, Riviere D, Kherif F, Boddaert N, Andrade A, Papadopoulos-Orfanos D, Poline J-B, Bloch I, Zilbovicius M, et al. 2003. A primal sketch of the cortex mean curvature: a morphogenesis based approach to study the variability of the folding patterns. *IEEE Trans Med Imaging*. 22:754–765. doi: 10.1109/TMI.2003.814781.

Chen C-H, Gutierrez ED, Thompson W, Panizzon MS, Jernigan TL, Eyler LT, Fennema-Notestine C, Jak AJ, Neale MC, Franz CE, et al. 2012. Hierarchical genetic organization of human cortical surface area. *Science*. 335:1634. doi: 10.1126/science.1215330.

Chi JG, Dooling EC, Gilles FH. 1977. Gyral development of the human brain. *Ann Neurol*. 1:86–93. doi: 10.1002/ana.410010109.

Chung MK, Worsley KJ, Robbins S, Paus T, Taylor J, Giedd JN, Rapoport JL, Evans AC. 2003. Deformation-based surface morphometry applied to gray matter deformation. *NeuroImage*. 18:198–213. doi: 10.1016/S1053-8119(02)00017-4.

Collins DL, Neelin P, Peters TM, Evans AC. 1994. Automatic 3D intersubject registration of MR volumetric data in standardized Talairach space. *J Comput Assist Tomogr*. 18:192–205.

Diogo MC, Prayer D, Gruber GM, Brugger PC, Stuhr F, Weber M, Bettelheim D, Kasprian G. 2019. Echo-planar FLAIR sequence improves subplate visualization in fetal MRI of the brain. *Radiology*. 292:159–169. doi: 10.1148/radiol.2019181976.

ten Donkelaar HJ, Kachlík D, Tubbs RS. 2018. *An illustrated terminologia neuroanatomica: a concise encyclopedia of human neuroanatomy*. Heidelberg: Springer.

Draganova R, Eswaran H, Murphy P, Huotilainen M, Lowery C, Preissl H. 2005. Sound frequency change detection in fetuses and newborns, a magnetoencephalographic study. *NeuroImage*. 28:354–361. doi: 10.1016/j.neuroimage.2005.06.011.

Dubois J, Benders M, Borradori-Tolsa C, Cachia A, Lazeyras F, Ha-Vinh Leuchter R, Sizonenko SV, Warfield SK, Mangin JF, Hüppi PS. 2008. Primary cortical folding in the human newborn: an early marker of later functional development. *Brain*. 131:2028–2041. doi: 10.1093/brain/awn137.

Duvernoy HM, Cabanis E-A, Iba-Zizen M-T, Tamraz J, Guyot J. 1992. *Le cerveau humain: surface, coupes sériées tridimensionnelles et IRM*, Springer-Verlag, Paris (1992), p. 358.

Eickhoff SB, Heim S, Zilles K, Amunts K. 2006. Testing anatomically specified hypotheses in functional imaging using cytoarchitectonic maps. *NeuroImage*. 32:570–582. doi: 10.1016/j.neuroimage.2006.04.204.

Fischl B, Rajendran N, Busa E, Augustinack J, Hinds O, Yeo BTT, Mohlberg H, Amunts K, Zilles K. 2008. Cortical folding patterns and predicting cytoarchitecture. *Cereb Cortex*. 1991:1973–1980. doi: 10.1093/cercor/bhm225.

Fogliarini C, Chaumoitre K, Chapon F, Fernandez C, Lévrier O, Figarella-Branger D, Girard N. 2005. Assessment of cortical maturation with prenatal MRI. Part I: normal cortical maturation. *Eur Radiol*. 15:1671–1685. doi: 10.1007/s00330-005-2782-1.

Garel C, Chantrel E, Brisse H, Elmaleh M, Luton D, Oury JF, Sebag G, Hassan M. 2001. Fetal cerebral cortex: normal gestational landmarks identified using prenatal MR imaging. *AJNR Am J Neuroradiol*. 22:184–189.

Garel C, Chantrel E, Elmaleh M, Brisse H, Sebag G. 2003. Fetal MRI: normal gestational landmarks for cerebral biometry, gyration and myelination. *Childs Nerv Syst ChNS Off J Int Soc Pediatr Neurosurg*. 19:422–425. doi: 10.1007/s00381-003-0767-4.

Habas PA, Scott JA, Roosta A, Rajagopalan V, Kim K, Rousseau F, Barkovich AJ, Glenn OA, Studholme C. 2012. Early folding patterns and asymmetries of the normal human brain detected from in utero MRI. *Cereb Cortex*. 1991:13–25. doi: 10.1093/cercor/bhr053.

Hasnain MK, Fox PT, Woldorff MG. 2001. Structure–function spatial covariance in the human visual cortex. *Cereb Cortex*. 1991:702–716.

Huang H, Xue R, Zhang J, Ren T, Richards LJ, Yarowsky P, Miller MI, Mori S. 2009. Anatomical characterization of human Fetal brain development with diffusion tensor magnetic resonance imaging. *J Neurosci*. 29:4263–4273. doi: 10.1523/JNEUROSCI.2769-08.2009.

Huotilainen M, Kujala A, Hotakainen M, Parkkonen L, Taulu S, Simola J, Nenonen J, Karjalainen M, Näätänen R. 2005. Short-term memory functions of the human fetus recorded with magnetoencephalography. *NeuroReport*. 16:81–84. doi: 10.1097/00001756-200501190-00019.

Im K, Choi YY, Yang J-J, Lee KH, Kim SI, Grant PE, Lee J-M. 2011a. The relationship between the presence of sulcal pits and intelligence in human brains. *NeuroImage*. 55:1490–1496. doi: 10.1016/j.neuroimage.2010.12.080.

Im K, Grant PE. 2019. Sulcal pits and patterns in developing human brains. *NeuroImage*. 185:881–890. doi: 10.1016/j.neuroimage.2018.03.057.

Im K, Guimaraes A, Kim Y, Cottrill E, Gagoski B, Rollins C, Ortinau C, Yang E, Grant PE. 2017. Quantitative folding pattern analysis of early primary sulci in human Fetuses with brain abnormalities. *AJNR Am J Neuroradiol*. 38:1449–1455. doi: 10.3174/ajnr.A5217.

Im K, Jo HJ, Mangin J-F, Evans AC, Kim SI, Lee J-M. 2010. Spatial distribution of deep sulcal landmarks and hemispherical asymmetry on the cortical surface. *Cereb Cortex*. 1991:602–611. doi: 10.1093/cercor/bhp127.

Im K, Lee J-M, Jeon S, Kim J-H, Seo SW, Na DL, Grant PE. 2013a. Reliable identification of deep sulcal pits: the effects of scan session, scanner, and surface extraction tool. *PloS One*. 8:e53678. doi: 10.1371/journal.pone.0053678.

Im K, Pienaar R, Lee J-M, Seong J-K, Choi YY, Lee KH, Grant PE. 2011b. Quantitative comparison and analysis of sulcal patterns using sulcal graph matching: a twin study. *NeuroImage*. 57:1077–1086. doi: 10.1016/j.neuroimage.2011.04.062.

Im K, Pienaar R, Paldino MJ, Gaab N, Galaburda AM, Grant PE. 2013b. Quantification and discrimination of abnormal sulcal patterns in polymicrogyria. *Cereb Cortex*. 1991:3007–3015. doi: 10.1093/cercor/bhs292.

Im K, Raschle NM, Smith SA, Ellen Grant P, Gaab N. 2016. Atypical sulcal pattern in children with developmental dyslexia and at-risk kindergarteners. *Cereb Cortex*. 1991:1138–1148. doi: 10.1093/cercor/bhu305.

Judaš M, Sedmak G, Kostović I. 2013. The significance of the subplate for evolution and developmental plasticity of the human brain. *Front Hum Neurosci*. 7:423. doi: 10.3389/fnhum.2013.00423.

Krsnik Ž, Majić V, Vasung L, Huang H, Kostović I. 2017. Growth of thalamocortical fibers to the somatosensory cortex in the human fetal brain. *Front Neurosci*. 11:233. doi: 10.3389/fnins.2017.00233.

Kuklisova-Murgasova M, Quaghebeur G, Rutherford MA, Hajnal JV, Schnabel JA. 2012. Reconstruction of fetal brain MRI with intensity matching and complete outlier removal. *Med Image Anal*. 16:1550–1564. doi: 10.1016/j.media.2012.07.004.

Le Guen Y, Auzias G, Leroy F, Noulhiane M, Dehaene-Lambertz G, Duchesnay E, Mangin J-F, Coulon O, Frouin V. 2017. Genetic influence on the sulcal pits: on the origin of the first cortical folds. *Cereb Cortex*. 1991:1–12. doi: 10.1093/cercor/bhx098.

Lohmann G, von Cramon DY, Colchester ACF. 2008. Deep sulcal landmarks provide an organizing framework for human cortical folding. *Cereb Cortex*. 1991(18):1415–1420. doi: 10.1093/cercor/bhm174.

Lohmann G, von Cramon DY, Steinmetz H. 1999. Sulcal variability of twins. *Cereb Cortex*. 1991(9):754–763.

Lyttelton O, Boucher M, Robbins S, Evans A. 2007. An unbiased iterative group registration template for cortical surface analysis. *NeuroImage*. 34:1535–1544. doi: 10.1016/j.neuroimage.2006.10.041.

Lyttelton OC, Karama S, Ad-Dab'bagh Y, Zatorre RJ, Carbonell F, Worsley K, Evans AC. 2009. Positional and surface area asymmetry of the human cerebral cortex. *NeuroImage*. 46:895–903. doi: 10.1016/j.neuroimage.2009.03.063.

MacDonald D, Kabani N, Avis D, Evans AC. 2000. Automated 3-D extraction of inner and outer surfaces of cerebral cortex from MRI. *NeuroImage*. 12:340–356. doi: 10.1006/nimg.1999.0534.

Marin-Padilla M. 1970. Prenatal and early postnatal ontogenesis of the human motor cortex: a Golgi study. I. The sequential development of the cortical layers. *Brain Res*. 23:167–183. doi: 10.1016/0006-8993(70)90037-5.

Meng Y, Li G, Lin W, Gilmore JH, Shen D. 2014. Spatial distribution and longitudinal development of deep cortical sulcal landmarks in infants. *NeuroImage*. 100:206–218. doi: 10.1016/j.neuroimage.2014.06.004.

Meyer M, Desbrun M, Schröder P, Barr AH. 2003. *Discrete differential-geometry operators for triangulated 2-manifolds, in: visualization and mathematics III*. *Mathematics and visualization*. Berlin, Heidelberg: Springer, pp. 35–57.

Miller JA, Ding S-L, Sunkin SM, Smith KA, Ng L, Szafer A, Ebbert A, Riley ZL, Royall JJ, Aiona K, et al. 2014. Transcriptional landscape of the prenatal human brain. *Nature*. 508:199–206. doi: 10.1038/nature13185.

Mrzljak L, Uylings HBM, Kostovic I, van Eden CG. 1988. Prenatal development of neurons in the human prefrontal cortex: I. A qualitative Golgi study. *J Comp Neurol*. 271:355–386. doi: 10.1002/cne.902710306.

O'Leary DDM, Chou S-J, Sahara S. 2007. Area patterning of the mammalian cortex. *Neuron*. 56:252–269. doi: 10.1016/j.neuron.2007.10.010.

Ono M, Kubik S, Abernathey CD. 1990. *Atlas of the cerebral sulci*. Thieme.

Ortinau CM, Rollins CK, Gholipour A, Yun HJ, Marshall M, Gagoski B, Afacan O, Friedman K, Tworetzky W, Warfield SK, et al. 2019. Early-emerging sulcal patterns are atypical in fetuses with congenital heart disease. *Cereb Cortex*. 29:3605–3616. doi: 10.1093/cercor/bhy235.

Paus T, Tomaiuolo F, Otaky N, MacDonald D, Petrides M, Atlas J, Morris R, Evans AC. 1996. Human cingulate and paracingulate sulci: pattern, variability, asymmetry, and probabilistic map. *Cereb Cortex*. 6:207–214. doi: 10.1093/cercor/6.2.207.

Piao X, Hill RS, Bodell A, Chang BS, Basel-Vanagaite L, Straussberg R, Dobyns WB, Qasrawi B, Winter RM, Innes AM, et al. 2004. G protein-coupled receptor-dependent development of human frontal cortex. *Science*. 303:2033–2036. doi: 10.1126/science.1092780.

Rakic P. 2004. Genetic control of cortical convolutions. *Science*. 303:1983–1984. doi: 10.1126/science.1096414.

Robbins SM. 2004. *Anatomical standardization of the human brain in euclidean 3-space and on the cortical 2-manifold*. Canada: McGill University.

Ronan L, Fletcher PC. 2015. From genes to folds: a review of cortical gyrification theory. *Brain Struct Funct*. 220:2475–2483. doi: 10.1007/s00429-014-0961-z.

Rubenstein JLR, Rakic P. 1999. Genetic control of cortical development. *Cereb Cortex*. 9:521–523. doi: 10.1093/cercor/9.6.521.

Serag A, Aljabar P, Ball G, Counsell SJ, Boardman JP, Rutherford MA, Edwards AD, Hajnal JV, Rueckert D. 2012. Construction of a consistent high-definition spatio-temporal atlas of the developing brain using adaptive kernel regression. *Neuroimage*. 59:2255–2265. doi: 10.1016/j.neuroimage.2011.09.062.

Sled JG, Zijdenbos AP, Evans AC. 1998. A nonparametric method for automatic correction of intensity nonuniformity in MRI data. *IEEE Trans Med Imaging*. 17:87–97. doi: 10.1109/42.668698.

Stahl R, Walcher T, De Juan Romero C, Pilz GA, Cappello S, Irmler M, Sanz-Aquela JM, Beckers J, Blum R, Borrell V, et al. 2013. Trnp1 regulates expansion and folding of the mammalian cerebral cortex by control of radial glial fate. *Cell*. 153:535–549. doi: 10.1016/j.cell.2013.03.027.

Tao X, Prince JL, Davatzikos C. 2002. Using a statistical shape model to extract sulcal curves on the outer cortex of the human brain. *IEEE Trans Med Imaging*. 21:513–524. doi: 10.1109/TMI.2002.1009387.

Tarui T, Madan N, Farhat N, Kitano R, Ceren Tanritanir A, Graham G, Gagoski B, Craig A, Rollins CK, Ortinau C, et al. 2018. Disorganized patterns of sulcal position in fetal brains with agenesis of corpus callosum. *Cereb Cortex*. 28:3192–3203. doi: 10.1093/cercor/bhx191.

Vasung L, Huang H, Jovanov-Milošević N, Pletikos M, Mori S, Kostović I. 2010. Development of axonal pathways in the human fetal fronto-limbic brain: histochemical characterization and diffusion tensor imaging: axonal pathways in the human fetal brain. *J Anat*. 217:400–417. doi: 10.1111/j.1469-7580.2010.01260.x.

Vasung L, Lepage C, Radoš M, Pletikos M, Goldman JS, Richiardi J, Raguž M, Fischi-Gómez E, Karama S, Huppi PS, et al. 2016. Quantitative and qualitative analysis of transient fetal compartments during prenatal human brain development. *Front Neuroanat*. 10:11. doi: 10.3389/fnana.2016.00011.

Vasung L, Raguz M, Kostovic I, Takahashi E. 2017. Spatiotemporal relationship of brain pathways during human Fetal development using high-angular resolution diffusion MR imaging and histology. *Front Neurosci*. 11:348. doi: 10.3389/fnins.2017.00348.

Welker W. 1990. *Why does cerebral cortex fissure and fold?* Boston, MA: Springer, pp. 3–136.

Yun HJ, Chung AW, Vasung L, Yang E, Tarui T, Rollins CK, Ortinau CM, Grant PE, Im K. 2019. Automatic labeling of cortical sulci for the human fetal brain based on spatio-temporal information of gyrification. *NeuroImage*. 188:473–482. doi: 10.1016/j.neuroimage.2018.12.023.

Yun HJ, Im K, Yang J-J, Yoon U, Lee J-M. 2013. Automated sulcal depth measurement on cortical surface reflecting geometrical properties of sulci. *PloS One*. 8:e55977. doi: 10.1371/journal.pone.0055977.

Zijdenbos A, Evans A, Riahi F, Sled J, Chui J, Kollokian V. 1996. Automatic quantification of multiple sclerosis lesion volume using stereotaxic space. In: Höhne KH, Kikinis R, editors. *Visualization in biomedical computing, lecture notes in computer science*. Berlin Heidelberg: Springer, pp. 439–448.

Zilles K. 2018. Brodmann: a pioneer of human brain mapping—his impact on concepts of cortical organization. *Brain*. 141:3262–3278. doi: 10.1093/brain/awy273.

Zilles K, Schleicher A, Langemann C, Amunts K, Morosan P, Palomero-Gallagher N, Schormann T, Mohlberg H, Bürgel U, Steinmetz H, et al. 1997. Quantitative analysis of sulci in the human cerebral cortex: development, regional heterogeneity, gender difference, asymmetry, intersubject variability and cortical architecture. *Hum Brain Mapp*. 5:218–221. doi: 10.1002/(SICI)1097-0193(1997)5:4<218::AID-HBM2>3.0.CO;2-6.